

Metal-Organic Frameworks as stationary phases for mixed-mode separation applications

Chris S. Hawes, Yada Nolvachai, Chadin Kulsing, Gregory P. Knowles, Alan L. Chaffee, Philip J.

Marriott,* Stuart R. Batten* and David R. Turner*

Supporting Information

Index

- 2** Table of analyte parameters and retention values
- 3-4** Plots of analyte retention *versus* polarity, length and width
- 5-6** Structural analysis of compound 1B
- 7-9** Experimental Section
- 10** X-ray powder diffraction patterns for 1A and 1B
- 11** Thermogravimetric analysis for fresh and solvent-exchanged 1B
- 12-13** Discussion of separation method
- 14-16** Gas sorption experiments
- 17** References

Table S1 Analyte parameters for size selective and polar interaction studies, using H₆L1•2Cl•2H₂O, CdCO₃, and MOFs **1A** and **1B** packed in tips.

Analyte	Dipole ^a	Dimension ^a		Ligand	Retention ^b		
		W	L		CdCO ₃	1A	1B
Naphthalene	0	4.98	6.76	0	0	0.19	0.16
Acenaphthene	0.9758	5.90	6.79	0	0	0	0
Acenaphthylene	0.3595	6.19	6.80	0	0	0.07	0.05
Fluorene	0.5681	5.03	9.06	0	0.01	0.18	0.27
Anthracene	0	4.99	9.22	0	0.02	0.55	0.18
Phenanthrene	0.0147	5.57	9.30	0	0.02	0.63	0.37
Pyrene	0.0001	6.81	9.23	0	0.02	0.41	0
Fluoranthene	0.3501	6.80	8.67	0	0.02	0.50	0.11
Chrysene	0.0002	6.13	11.50	0	0.02	2.26	3.23
Benz[<i>a</i>]anthracene	0.0344	6.39	11.44	0	0.02	2.07	0.54
Benzo[<i>b</i>]-fluoranthrene	0.3904	7.54	11.41	0	0.02	1.29	0.60
Benzo[<i>k</i>]-fluoranthrene	0.2982	6.80	11.13	0	0.02	1.14	0.52
Benzo[<i>a</i>]pyrene	0.0107	7.16	11.40	0	0.02	1.66	1.06
Benzo[<i>ghi</i>]perylene	0.0407	8.02	9.32	0	0.02	3.37	0.27
Indeno[1,2,3- <i>cd</i>]-pyrene	0.6477	7.83	11.37	0	0.59	2.27	0.07
Dibenz[<i>a,h</i>]-anthracene	0.0006	6.55	13.59	0	0.01	2.07	1.76
Phenol	1.3941	4.34	5.64	0	0.67	2.08	1.57
Benzylalcohol	1.8430	4.73	7.00	0	0.78	2.04	1.56
Phenylethanol	1.8119	4.37	7.08	0	0.95	1.50	1.56
Pantolactone	3.8558	4.38	5.64	0.33	0.95	2.65	2.16
Phenylpropanol	1.9272	4.18	8.11	0	0.95	1.85	1.76
Naphthalene	0	4.98	6.76	0	0	0.12	0.10
Benzamide	3.7911	4.32	7.10	0	2.18	2.85	2.33
Phenanthrene	0.0147	5.57	9.30	0	0.02	1.08	0.57
Caffeine	4.0612	6.22	7.46	1.78	0.92	3.42	2.62
4,4'-Biphenol	0.0188	4.32	10.67	2.33	1.74	3.04	2.10

Pyrene	0.0001	6.81	9.23	0	0.02	1.31	0.22
Bisphenol A	0.9729	5.53	9.48	2.33	1.70	3.23	2.41

^a Parameters obtained from GAUSSIAN09¹, using B3LYP 6-311++G(d,p) basis set. Dipole moment values are expressed as debye (D). Dimensions, width (W) and length (L) are inter-atomic distances, expressed in angstrom (Å) units. ^bRelative to acenaphthene. PAH elution was carried out by stepwise gradient 100% EtOAc – 50% EtOAc/Hexane, and polar compounds by 50% EtOAc/Hexane - 100% EtOAc

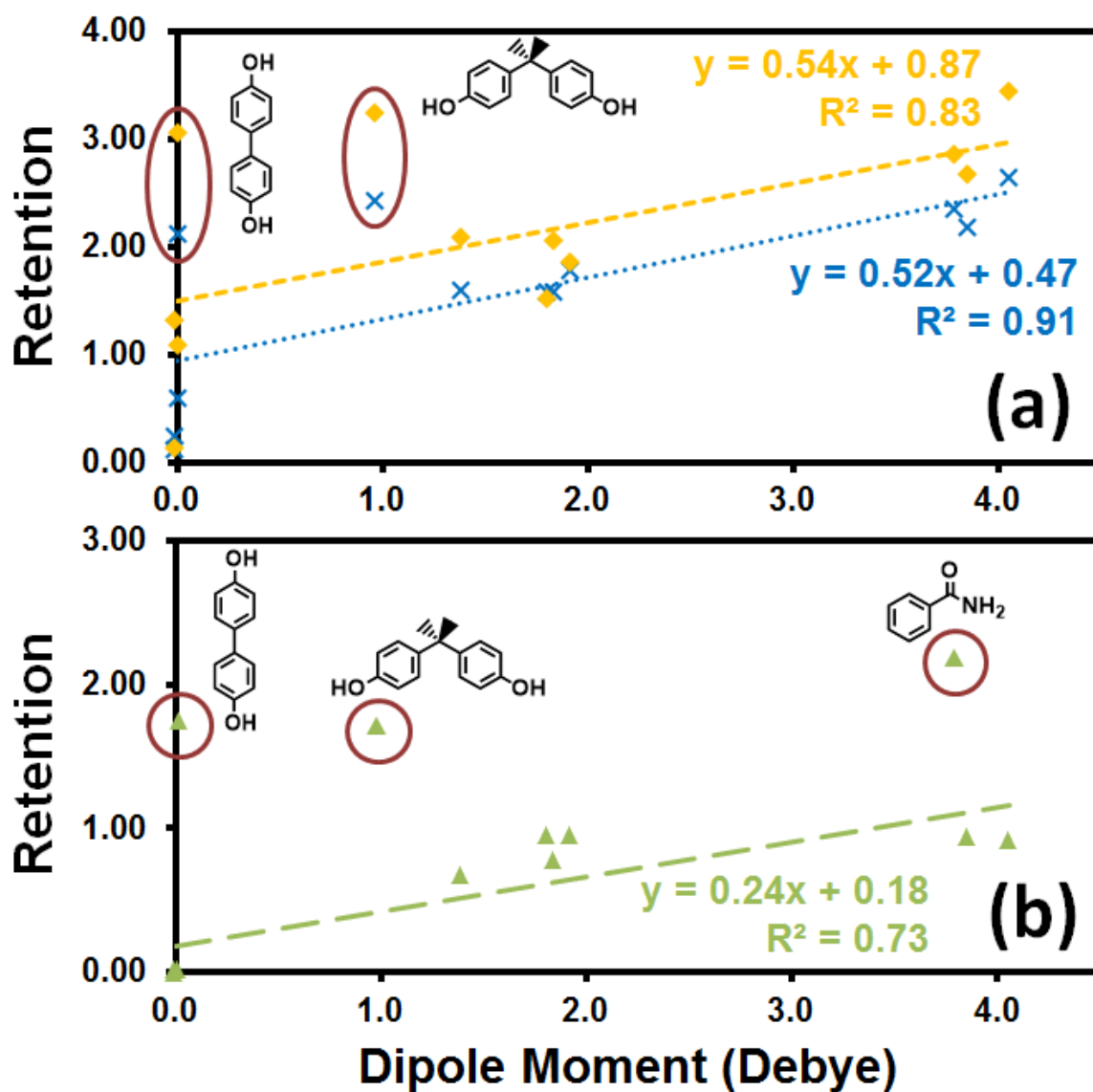


Figure S1 (a) Correlations of polar analyte retention and their dipole moment using **1A** and **1B** packed tips (diamonds and crosses, respectively). (b). Dipole moment correlation using CdCO₃-packed tips. The corresponding values are shown in Table 1. Linear equations were

calculated without the highlighted analytes, which were suspected to undergo hydrogen bonding and/or metal coordination as well as dipole effects.

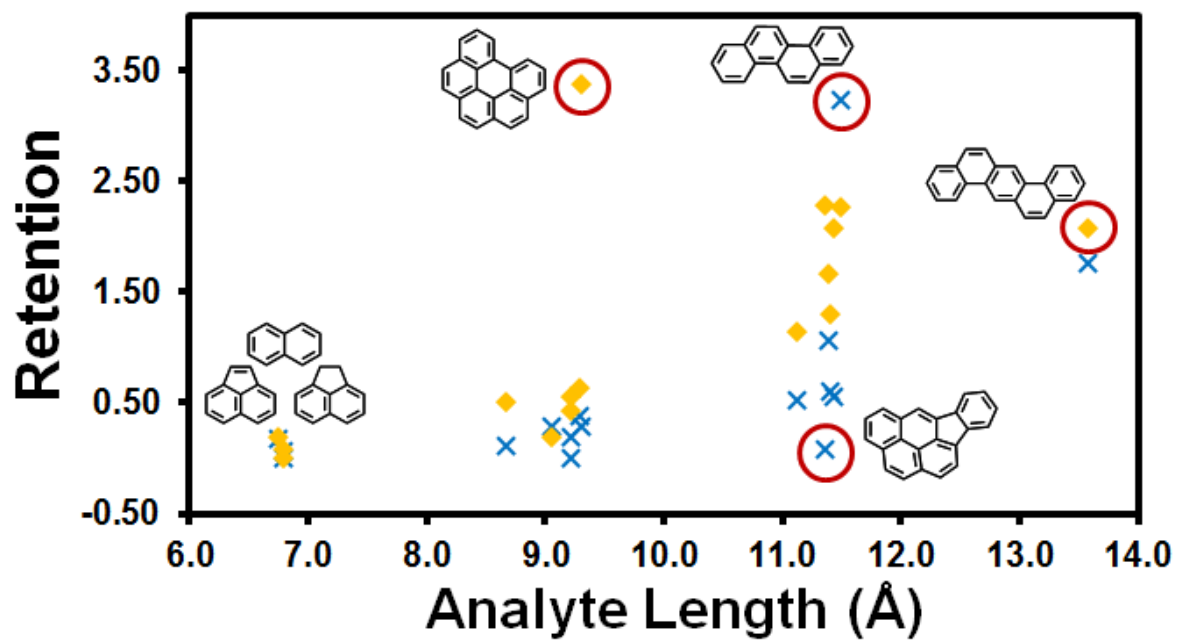


Figure S2: Plot of retention versus analyte length for compounds **1A** (yellow) and **1B** (blue). Analytes which fall outside the general trend of increasing retention with length are circled in red.

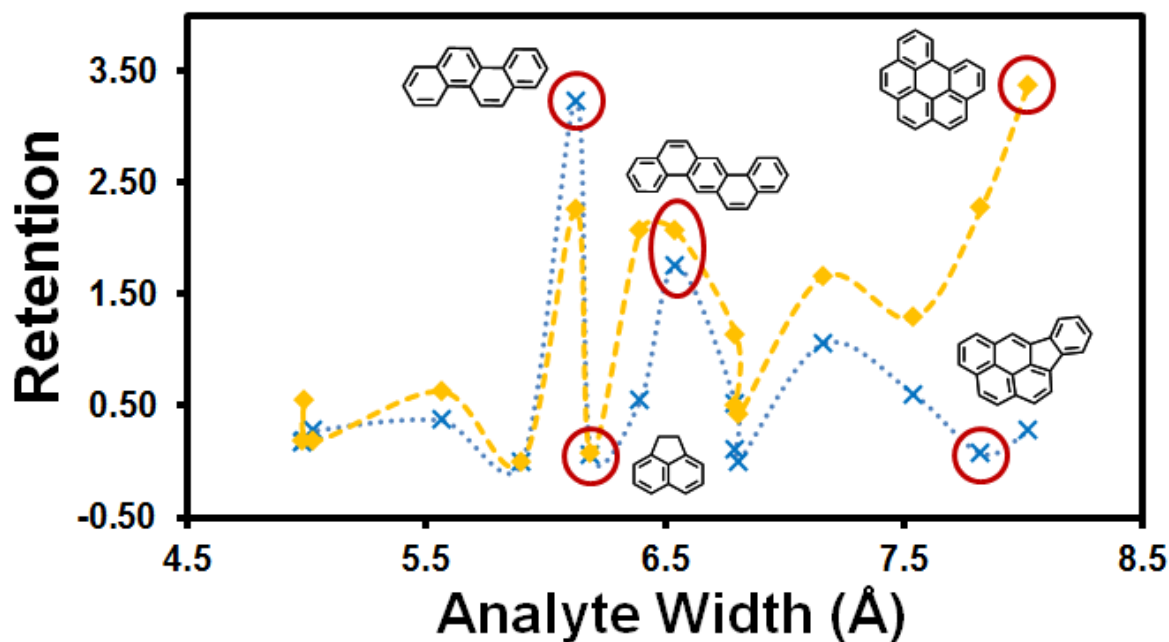


Figure S3: Plot of retention versus analyte width for compounds **1A** (yellow) and **1B** (blue). Representative example compounds are circled in red and structures shown for reference.

Structural Analysis of 1B

The structure displayed a doubly-interpenetrated 3,4-connected binodal topology, containing two Cd(II) sites - one encapsulated within the macrocyclic cavity with a chelating carboxylate group in the axial position, with an overall +1 charge, and the second engaged in a tris-carboxylate chelate coordination mode, displaying a -1 charge (Figure S4). This results in an overall neutral framework with pseudo-zwitterionic character. The interpenetration allows the networks to associate such that electrostatic contacts between frameworks are maximised ($\sim 6\text{\AA}$ between +1 and -1 charges from adjacent frameworks), while retaining porosity.

The four arms of the ligand are splayed out in a roughly square planar conformation, so that each arm connects to a different cadmium atom, three being Cd atoms bound by three carboxylates and thus acting as 3-connecting nodes, and the other to a macrocyclic-bound Cd. These structural features are shared by both **1A** and **1B**. The coordination of the macrocyclic

Cd by a carboxylate arm from an adjacent macrocycle leads to the CdL1 species acting as 5-connecting nodes, to generate an overall 3,5-connected **kdd** net. By contrast, in **1A** one of the arms is twisted out of the plane of the others.² This arm coordinates to the metal in the centre of an adjacent macrocycle, and this second macrocycle reciprocates the interaction with its own out-of-plane benzoate arm, leading to a double bridge which reduces the connectivity of the cadmium macrocycle node, generating a 3,4-connected **ins** net.

The topological differences between the two structures can be observed in Figure S5; MOF **1B** contains one additional link compared to **1A**, effectively reducing the size of the primary channels in **1B**.

Gao *et al.* reported the presence of a water molecule coordinating to the carboxylate-bound cadmium atom in **1A**.² Due in part to framework disorder and difficult diffraction characteristics, we were unable to locate an equivalent ligand bound to compound **1B**, however the presence of considerable quantities of solvent within the isolated material suggests that some solvent coordination to the Cd2 site is possible.

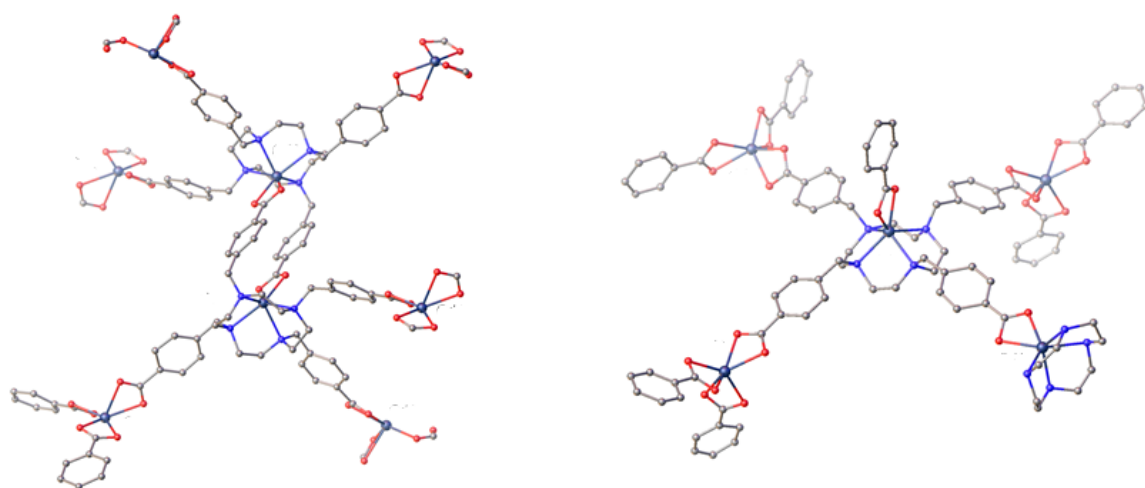


Figure S4: Comparison of chemical connectivity within the structures of **1A** (left) and **1B** (right), showing the effect of the pivot of one benzoate arm towards or away from the axial donor, respectively.

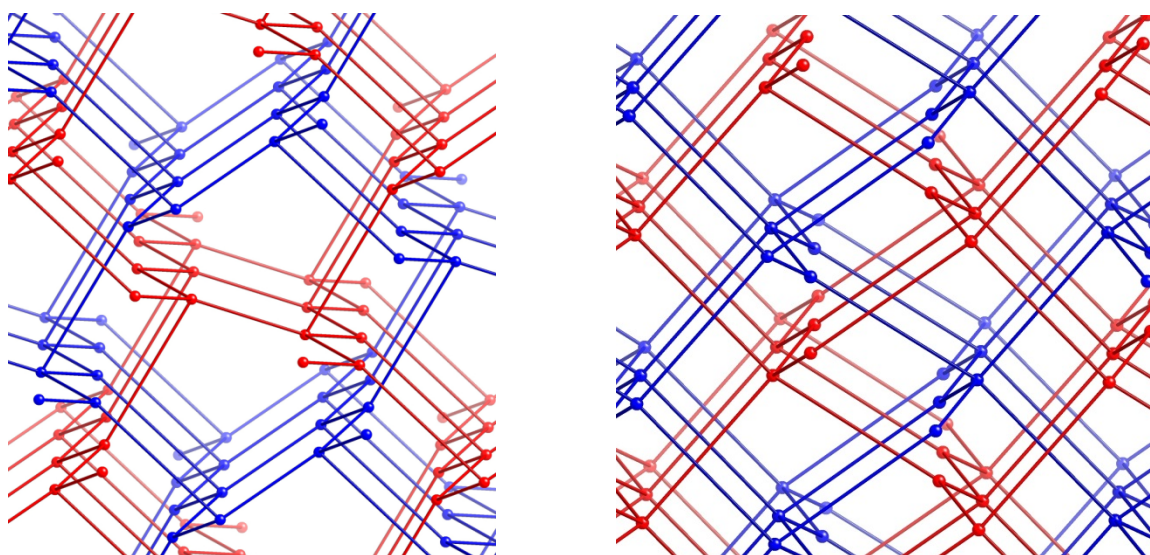


Figure S5: Topological comparison of MOFs **1A** (left) and **1B** (right), with independent networks coloured separately, and nodes representing cadmium ions with 3,4-connectivity (**1A**) or 3,5-connectivity (**1B**)

Experimental

Materials and Methods

Ethyl acetate (EtOAc), dimethylformamide and hexane (GC grade) were obtained from Merck KGaA. (Darmstadt, Germany). PAH mix (49156) was from Supelco (Bellafonte, PA, USA). Cadmium carbonate and all other compounds in **Table 1** were from Sigma Aldrich (St. Louis, MO, USA). Synthesis of $\text{H}_6\text{L1}\cdot 2\text{Cl}\cdot 2\text{H}_2\text{O}$ was carried out as previously described.³ Cadmium nitrate was obtained from Alfa Aesar. Melting points were recorded in air on an Electrothermal melting point apparatus, and are uncorrected. Microanalysis was performed by Campbell Microanalytical Laboratory, University of Otago, New Zealand. Infrared spectra were obtained using an Agilent Cary 630 spectrometer equipped with an Attenuated Total Reflectance (ATR) sampler. Thermogravimetric analysis was carried out using a Mettler-Toledo TGA/DSC 1 STARe system. Samples were heated at a rate of $5\text{ }^\circ\text{C min}^{-1}$ under a nitrogen purge flow of 30 ml min^{-1} . Bulk purity of all crystalline materials was

confirmed with powder X-ray diffraction (PXRD) patterns recorded with a Bruker X8 Focus powder diffractometer operating at Cu K α wavelength (1.5418 Å), with samples mounted on a zero-background silicon single crystal stage. Scans were performed at room temperature in the 2 θ range 5 – 55° and compared with predicted patterns based on single crystal data. Both materials were stable on standing in air after isolation from the reaction mixtures, although the presence of diffuse pore contents resulted in relatively poor PXRD intensity. On exchange of the non-volatile reaction solvent, no appreciable diffraction was observed, preventing any further PXRD analysis of the materials. As a precaution, during solvent exchange and separation experiments, both **1A** and **1B** were prevented from completely drying.

Synthesis of poly-[Cd(L1)]·8H₂O·5.5DMF 1B:

Cadmium nitrate tetrahydrate (16 mg, 52 μ mol) and H₆L1·2Cl·2H₂O (10 mg, 12 μ mol) were combined in 1 mL DMF and heated to 100 °C. The solution was allowed to stand for two days, giving colourless rod crystals which were filtered and dried in air. Yield 9 mg (51%). m.p. >300 °C; Found C, 45.77; H, 5.73; N, 9.17; calculated for C₄₀H₄₀N₄O₈Cd₂·8H₂O·5.5DMF C, 45.98; H, 6.46; N, 9.02%; TGA mass loss 35.4% (RT – 200 °C, one step), calculated for 8 H₂O 5.5 DMF 37.0%; ν_{\max} (ATR, cm⁻¹) 3422m br, 2925w, 2868w, 1652s, 1587m, 1540w, 1385s, 1253m, 1091m, 1064m, 945w. Crystallographic Data: C₄₀H₄₀Cd₂N₄O₈ (*M*=929.56): orthorhombic, space group *Cmca* (no. 64), crystal size 0.20x0.03x0.02 mm, *a* = 21.722(4) Å, *b* = 39.084(8) Å, *c* = 17.966(4) Å, *V* = 15253(5) Å³, *Z* = 8, *T* = 273 K, μ = 0.587 mm⁻¹ (λ = 0.7108 Å, synchrotron), *D*_{calc} = 0.810 g/mm³, 28405 reflections measured (3.12 ≤ 2 Θ ≤ 53.78), 8251 unique (*R*_{int} = 0.0830) which were used in all calculations. The final *R*₁ was 0.0787 (*I* > 2 σ (*I*), 5513 reflections) and *wR*₂ was 0.2524 (all

data, 8251 reflections). The SQUEEZE routine within PLATON⁴ was used to account for diffuse electron density within the solvent channels. CCDC 977250.

Synthesis of MOF-1A

A slight modification to the reported procedure was employed to prepare **1A** on a bulk scale, due to difficulties in reproducibility encountered from using the dihydrochloride salt of **L1** as a starting material. To H₆**L1**·2Cl·2H₂O (10 mg; 12 μmol) in a 200:1 mixture of N,N-dimethylacetamide: N-methyl pyrrolidinone (2 mL) was added cadmium nitrate tetrahydrate (16 mg; 52 μmol), and the mixture was sealed in a glass vial and heated to 120 °C for 16 h. The small, pale yellow crystals obtained were filtered and dried in air. Yield 4 mg. Phase purity was confirmed by X-ray powder diffraction (Figure S6)

X-Ray Crystallography

Data collection for compound **1B** was carried out at the Australian Synchrotron on the MX1 beamline, operating at 17.4 keV ($\lambda = 0.7108 \text{ \AA}$) with data collection conducted using BluIce control software.⁵ Corrected anomalous dispersion values were calculated where necessary using Brennan and Cowan data.⁶ The diffraction data were processed, reduced and corrected with the XDS software suite.⁷ The diffraction data were solved using direct methods with SHELXS⁸ and refined on F² using all data by full matrix least-squares procedures with SHELXL-97⁹ within OLEX 2.¹⁰ Non-hydrogen atoms were refined with anisotropic displacement parameters. Hydrogen atoms were modelled in calculated positions with isotropic displacement parameters 1.2 times the isotropic equivalent of their carrier atoms. The functions minimized were $\Sigma w(F_o^2 - F_c^2)$, with $w = [\sigma^2(F_o^2) + aP^2 + bP]^{-1}$, where $P = [\max(F_o)^2 + 2F_c^2]/3$. The structure was found to contain regions of diffuse electron density which were unable to be sensibly modelled, and as such, their contribution to the diffraction

data was accounted for with the SQUEEZE routine within PLATON,⁴ with assignment of encapsulated solvent molecules made on the basis of calculated electron count, thermogravimetric analysis and microanalysis. Attempts to collect diffraction data at the standard temperature of 100 K gave rise to a partial phase transition with symmetry lowering to an apparent *Pcca* setting, with significant loss of diffraction intensity to resolutions beyond ~ 1.2 Å. The diffraction data were therefore collected at 273 K, providing greatly improved resolution and a structure model in the space group *Cmca*. However, the structure still suffered from significant disorder and relatively poor diffraction characteristics commonly affecting porous materials containing flexible groups. The macrocyclic ring within the structure was found to be disordered across two equivalent orientations related by a bisecting mirror plane. This disorder was found to be present even when the data were modelled in lower symmetry space groups containing no bisecting symmetry elements and is most likely due to thermal motion of the flexible ring system. Presence of an aqua ligand coordinating to Cd₂ was suspected based on the structure of **1A**, however the Fourier difference peaks in this region were sufficiently diffuse to be inconclusive, and the model was not improved by the placement of a fully or partially occupied oxygen atom at a sensible coordinating position.

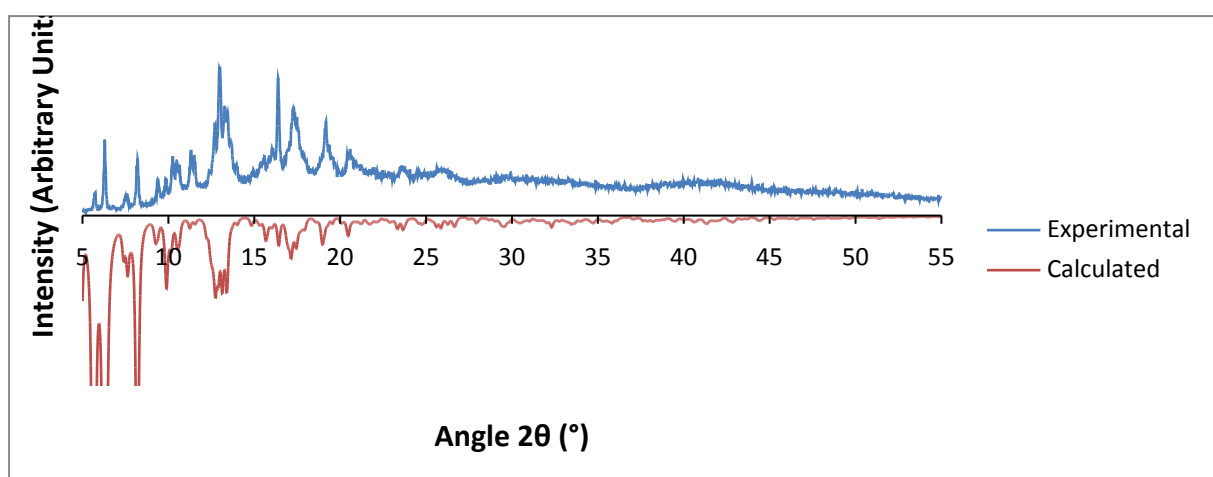


Figure S6: Comparison of experimental and calculated X-ray powder diffraction patterns for **1A**.

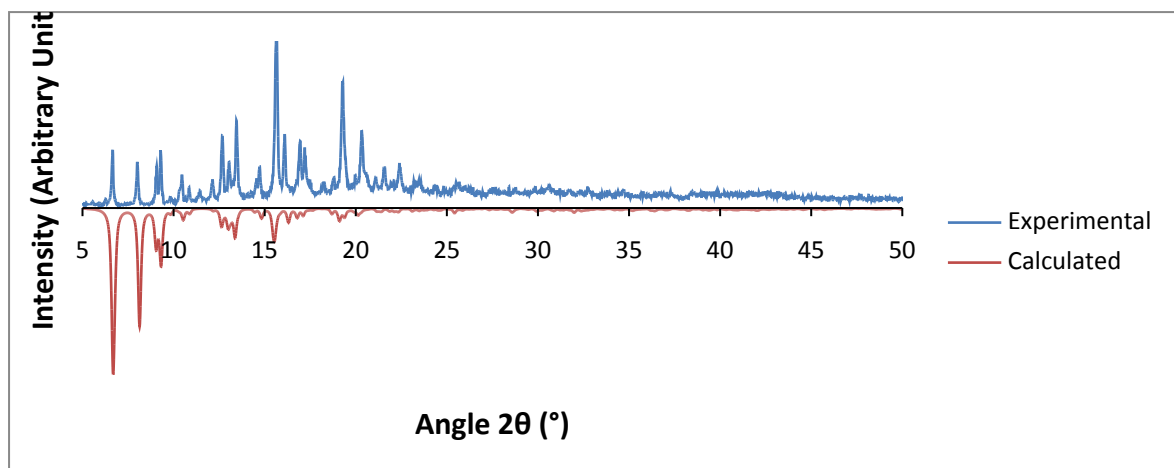


Figure S7: Comparison of experimental and calculated X-ray powder diffraction patterns for **1B**.

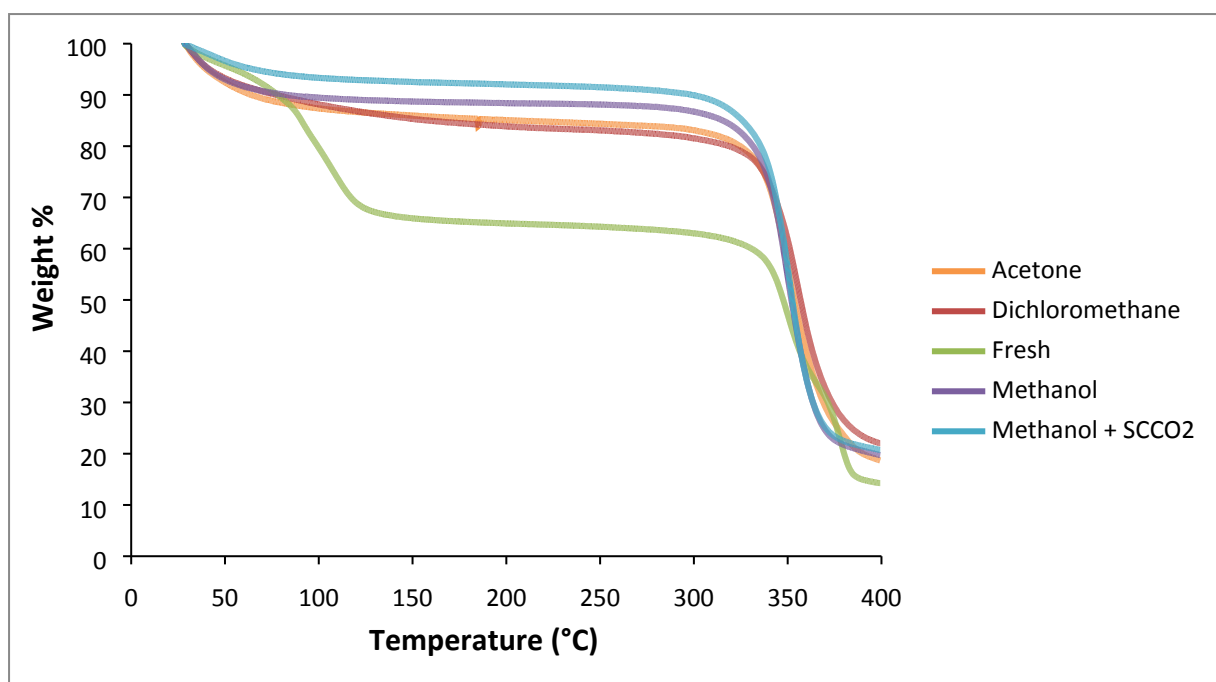


Figure S8: Thermogravimetric analysis traces for **1B**, for freshly isolated sample (green), samples soaked for two days in acetone (orange), dichloromethane (red) and methanol (purple), and supercritical CO₂-activated methanol-soaked sample (blue).

Separation in Tips

PAH and polar compound mixtures were prepared in EtOAc and hexane, respectively, using commercially available mixtures. Four separate micro-pipette tips were packed with freshly prepared MOFs **1A** and **1B**, CdCO₃ and the ligand dihydrochloride hydrate (60 mg each) under pressure for 5 min (Figure S10). The tips were flushed with 500 μL of DMF and soaked in DMF for another 2 h. Before loading, each tip was equilibrated with 100% v/v EtOAc or 100% v/v hexane for PAH or polar separation (respectively). Solutions of the PAH mixture or polar compound mixture (10 μL) were loaded into each tip for the separation study. For PAH separation, 100% v/v EtOAc solution was applied as the eluent from 0-30 min. The eluent was changed to 50% v/v EtOAc/hexane after 30 min. For polar separation, 50% v/v EtOAc/hexane solution was applied as the eluent from 0-30 min. The eluent was changed to 100% EtOAc after 30 min. Each 30 μL of the collected fraction from the tips (corresponding to 5 min eluate time) was simply controlled by the use of a pressurised disposable syringe. All fractions were transferred into vials for GC analysis. The retention volume for each analyte given by the maximum of the peak area plot was identified assuming

Gaussian peak shape, and retention was then calculated from the relative retention volume (Table S1). Gaussian peak shapes could not be applied for analytes displaying highly asymmetric distribution, such as benzo[*k*]fluoranthene (Manuscript, Figure 2a). In this case, the elution volume corresponding to the maximum peak intensity was selected to be the retention volume. It should be noted that the separation of non-polar analytes (PAHs) was improved by firstly using a more polar mobile phase (ethyl acetate) eluting unretained analytes followed by a less polar mobile phase (hexane/ethyl acetate) eluting the rest, as is standard strategy for reverse phase chromatography. Conversely, polar analyte separation was improved by using a non-polar mobile phase (hexane) eluting unretained analytes followed by the more polar mobile phase (ethyl acetate/hexane) eluting the rest, as standard for the concept of normal phase chromatography.

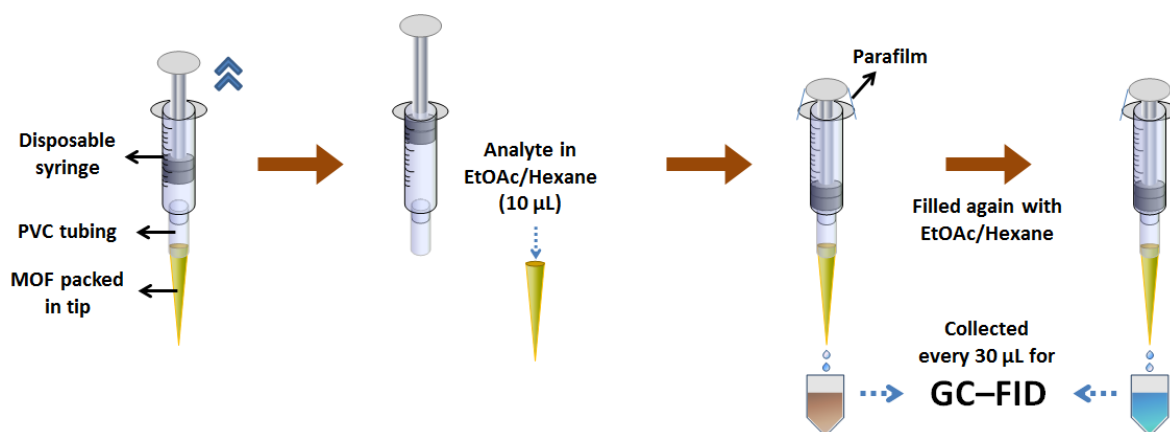


Figure S9: Schematic diagram of tip separation protocol

Analyte solutions (1 µL, split ratio of 5:1 for PAH and 20:1 for polar compounds) were injected into an Agilent 6850 GC (Agilent Technologies, Mulgrave, Australia) coupled with FID, installed with an Rxi®-17Sil MS column of 15 m × 0.18 mm × 0.18 µm film thickness (Restek, Bellefonte, PA). For PAH, the oven temperature program was set at 50 °C, heated to

260 °C at 25 °C min⁻¹, and finally to 280 °C at 5 °C min⁻¹ (held for 5 min), while for polar compounds the program started at 40 °C, ramped to 150 °C at 20 °C min⁻¹ and to 320 °C at 25 °C min⁻¹ (held for 5 min). Hydrogen was used as the carrier gas at a flow rate of 0.5 mL min⁻¹. Injector and detector temperatures were 320 °C and 300 °C respectively. Data were collected at 20 Hz. Data acquisition and analysis was performed using ChemStation software.

Gas Sorption Experiments

A sample of compound **1B** (~150 mg) was soaked in 20 mL of methanol for 3 days, with the solvent decanted and replaced with fresh methanol every 24 h. Following this period, the solids were filtered and subjected to supercritical CO₂ exchange using a Tousimis Samdri PVT-3D instrument. Liquid CO₂ was passed across the material within porous Teflon cups for 2 h, after which the chamber pressure and temperature were increased above the critical point, and allowed to dwell for 4 h. The chamber was purged to atmospheric pressure, and the process was repeated once more. Immediately following the completion of the exchange cycle, the sample was loaded into a standard glass bulb sample tube, which was evacuated at room temperature overnight using a Micromeritics VacPrep 061 Degasser instrument to prepare it for gas sorption analysis. The sample was analysed for carbon dioxide and nitrogen uptake, at 273 K and 77 K, respectively, using a Micromeritics Tristar 3020 instrument. Ultra high purity gasses (AirLiquide) were used for all analyses. MOF **1B** was found to uptake only minimal quantities of N₂ up to the saturation pressure at 77 K under the experimental conditions, and as such, nitrogen was not considered a useful probe gas for this material.

Similar behaviour was observed by Gao *et al.* for compound **1A**.^[2] Surface area was calculated from the CO₂ data using both the BET and Dubinin-Radushkevitch models within the Tristar 3020 V1.03 Software, using datapoints in the range $P/P_0 = 0.01 - 0.025$ for BET and using all datapoints for DR (Figures **S10** and **S11**). The surface area values obtained were 141 and 204 m² g⁻¹ for BET and DR, respectively.

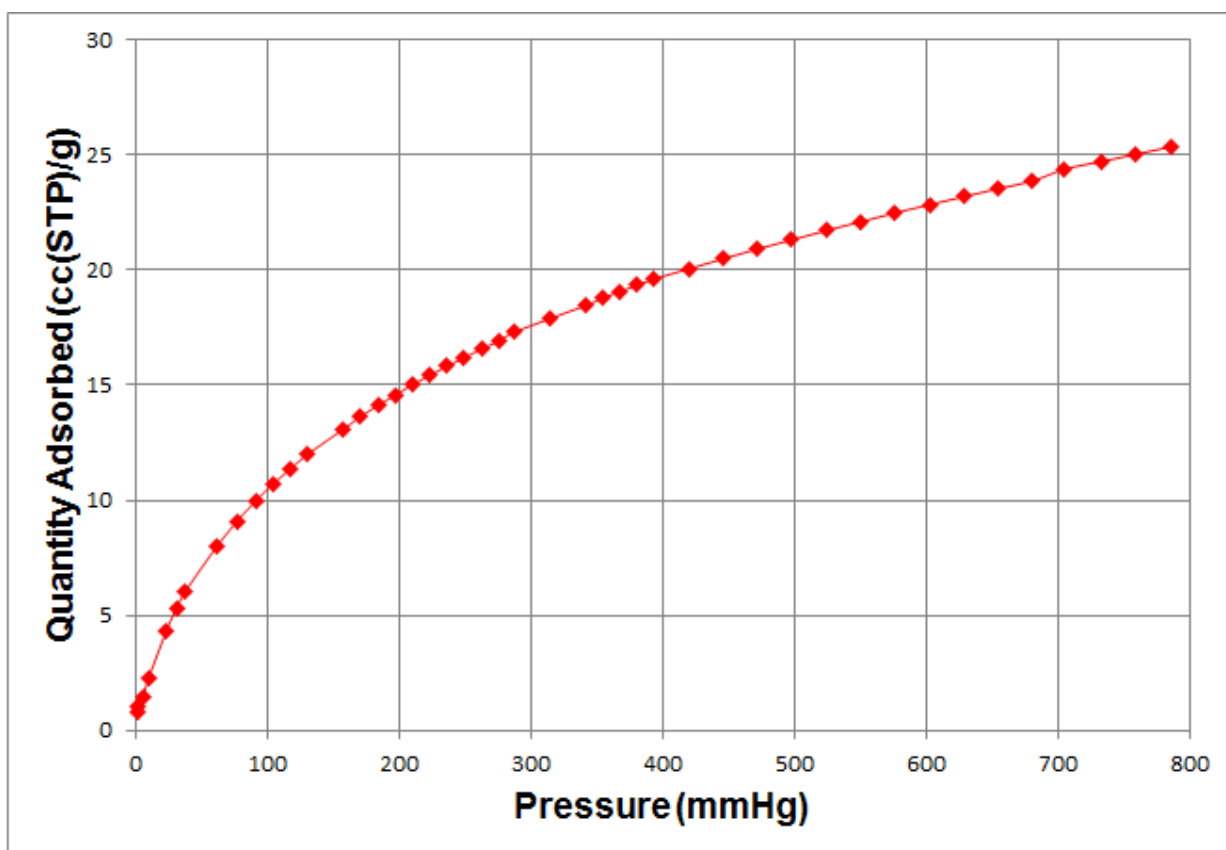


Figure S9: CO₂ sorption isotherm plot for **1B**, measured at 273K

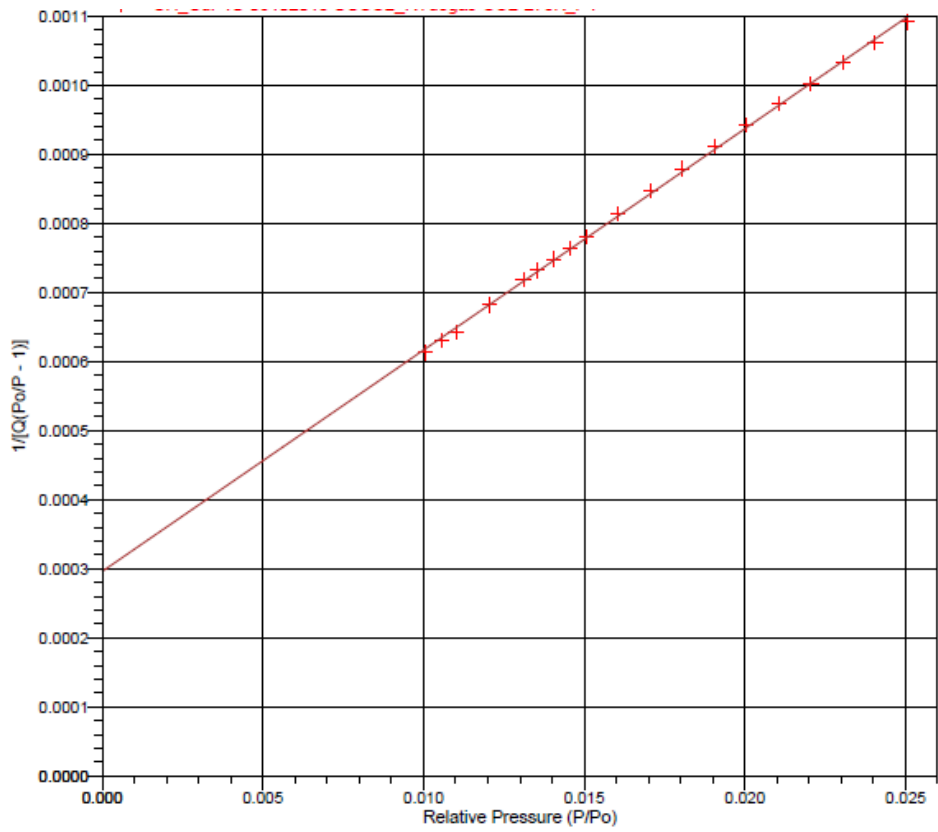


Figure S10: BET Surface Area plot for **1B**

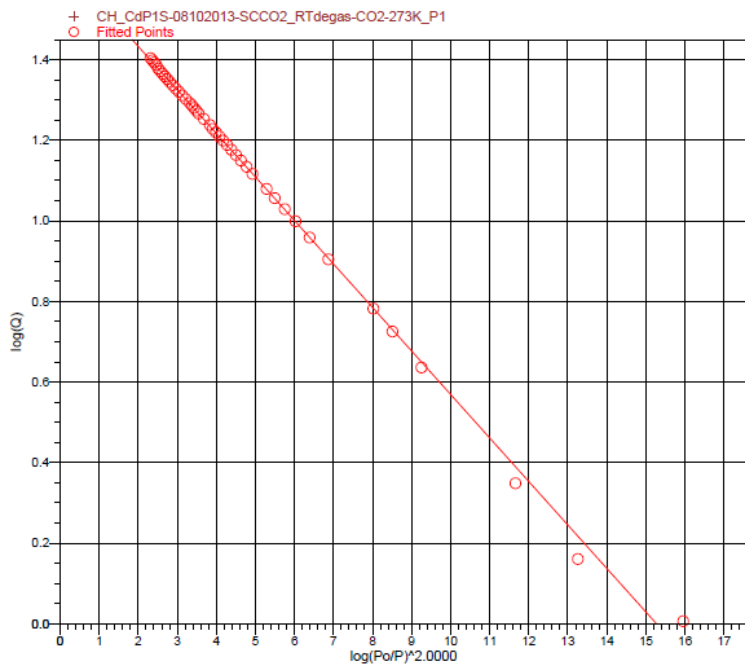


Figure S11: Dubinin-Radushkevitch Transformed Isotherm plot

References

- 1 M. J. Frisch, G. W. Trucks, H. B. Schlegel *et al.*, *Gaussian09, Revision A.02*, Gaussian Inc., Wallingford, CT, 2009.
- 2 W.-Y. Gao, Y. Niu, Y. Chen, L. Wojtas, J. Cai, Y.-S. Chen, S. Ma, *CrystEngComm*, 2012, **14**, 6115-6117
- 3 C. S. Hawes, S. R. Batten, D. R. Turner, *CrystEngComm*, In Press, DOI:10.1039/C3CE42141D
- 4 A. L. Spek, *Acta Crystallogr. Sect. D.*, 2009, **65**, 148–155; P. v.d. Sluis and A. L. Spek, *Acta Crystallogr. Sect. A.*, 1990, **46**, 194-201
- 5 T. M. McPhillips, S. E. McPhillips, H.-J. Chiu, A. E. Cohen, A. M. Deacon, P. J. Ellis, E. Garman, A. Gonzalez, N. K. Sauter, R. P. Phizackerly, S. M. Soltis and P. Kuhn, *J. Synchrotron Rad.*, 2002, **9**, 401-406

- 6 S. Brennan and P. L. Cowan, *Rev. Sci. Instrum.*, 1992, **63**, 850-853
- 7 W. J. Kabsch, *J. Appl. Cryst.*, 1993, **26**, 795-800.
- 8 G. M. Sheldrick, *Acta Crystallogr. Sect. A.*, 2008, **64**, 112–122.
- 9 G. M. Sheldrick, *SHELXL-97, Programs for X-ray Crystal Structure Refinement*; University of Göttingen: Göttingen, Germany, 1997.
- 10 O. V. Dolomanov, L. J. Bourhis, R. J. Gildea, J. A. K. Howard, H. Puschmann, *J. Appl. Cryst.*, 2009, **42**, 339-341